STUDIA UBB CHEMIA, LXV, 2, 2020 (p. 171-186)
(RECOMMENDED CITATION)
DOI:10.24193/subbchem.2020.2.14

CHARACTERIZATION AND APPLICATION OF NEW EFFICIENT NANOSORBENT Fe_2O_3 PREPARED BY A MODIFIED LOW-TEMPERATURE UREA METHOD

MILJANA RADOVIĆ VUČIĆ[a*], JELENA MITROVIĆ[a], MILOŠ KOSTIĆ[a], NENA VELINOV[a], SLOBODAN NAJDANOVIĆ[a], DANIJELA BOJIĆ[a], ALEKSANDAR BOJIĆ[a]

ABSTRACT. In this work, low-cost non-conventional nanostructured Fe_2O_3 was produced by a modified low-temperature urea method (MLTUM-Fe_2O_3). Non-magnetic amorphous nanoparticle MLTUM-Fe_2O_3 with a bouquet like morphology is found to play as an effective sorbent media to remove textile dye Reactive Blue 19 from textile industries dye effluents over a wide range of pH. The nanoparticles were characterized by X-ray powder diffraction analysis (XRD), scanning electron microscopy (SEM), energy dispersive X-ray spectroscopy (EDX), FTIR and TGA. The surface area was measured by Brunauer-Emmett-Teller (BET) analysis. SEM image reveals bouquet like morphology with average particle size about 50 nm. The maximum sorption capacity of the sorbent is found to be 271.00 mg g^{-1} for Reactive Blue 19 and the data fitted with different isotherm models. Study on sorption kinetics shows that sorption of Reactive Blue 19 onto iron oxide follows pseudo-second-order kinetic.

Keywords: *Amorphous materials, Nanostructures, Iron oxide, Chemical synthesis, Thermogravimetric analysis (TGA), X-ray diffraction*

INTRODUCTION

One of the most important industries using synthetic dyes is the textile and garment, which produces a strongly colored wastewater, typically with a concentration in the range of 10–200 mg dm^{-3} [1,2]. During the dyeing process, the competition between the colouring reaction and the hydrolysis of the reactive group results in a loss of unfixed dye of approximately 20–

[a] *The University of Niš, Faculty of Sciences and Mathematics, Department of Chemistry, Višegradska 33, 18 000 Niš, Serbia*
** Corresponding author: mimaradovic@gmail.com*

25% [3], thus leading to the production of coloured effluents [4,5]. Reactive Blue 19 (RB 19) dye is commonly used in the textile and leather industry and may be mutagenic and toxic because of the presence of electrophilic vinylsulfone groups [6,7].

Sorption is one of the most powerful methods for the removal of various forms of wastewater contaminants [8–12]. High efficiency, non-toxic, simplicity and low cost, have made the sorption processes preferable among the other conventional methods. A lot of studies have been reported on the kinetics, equilibrium and thermodynamics of various classes of dyes sorption onto numerous synthetic and natural sorbents, including activated carbon, biomaterials, silica, MgO, chitosan, peat, clay, bentonite and feather [13–27]. There are few papers that describe the RB 19 dye sorption on metal oxides. Table S1 in Supplementary material section shows a summary of some sorbents for the removal of RB 19 from wastewater.

Among numerous metal oxides, iron oxide has been paid intensive attention due to its stability, eco-friendly, high efficiency non-toxic and inexpensive nature. In this study, a new nanosorbent based on Fe_2O_3 was prepared using a modified low-temperature urea method. For practical application of Fe_2O_3 produced by a modified low-temperature urea method (MLTUM-Fe_2O_3) for treatment of dye contaminated wastewater, it is important to determine the optimal experimental conditions. The present work involves the effects of parameters, such as pH, sorbent dose, and sorbate concentration on RB 19 dye removal, the kinetic and equilibrium studies of RB 19 dye sorption onto MLTUM-Fe_2O_3. Desorption of RB19 and reused of MLTUM-Fe_2O_3 nanosorbent are also done.

RESULTS AND DISCUSSIONS

Characterization and sorption study

To analyse and quantify the pore structure and surface area of the obtained sorbent, the N_2 adsorption-desorption isotherms were carried out and shown in Fig. S3 in Supplementary material section (a). The pore size distribution, calculated via BJH method based on desorption curve, is presented in Fig. S3 in Supplementary material section (b). The sample has a BET surface area of 206.9 $m^2\ g^{-1}$. The measured micropore (pores below 2 nm) area by the t-plot method was 30 $m^2\ g^{-1}$. The micropore volume was 0.011911 $cm^3\ g^{-1}$, while the pore volume in range of 1.7 to 300 nm was 0.205275 $cm^3\ g^{-1}$. The average pore size was 4.1378 nm. A high surface area and mesoporous nature of MLTUM-Fe_2O_3 would be beneficial to sorb more organic pollutants on its surface.

Figure 1 presents the SEM images of MLTUM-Fe_2O_3. It can be seen that the surface is porous in nature. The sorbent particles are irregular in respect of size and shape. The sample consisted of particles below 5 μm in size with a textured structure of 100 nm which were elongated. The EDX results are presented in Fig. 2. The sample consisted of Fe and O only.
XRD showed that the sample is amorphous with no crystalline fractions.

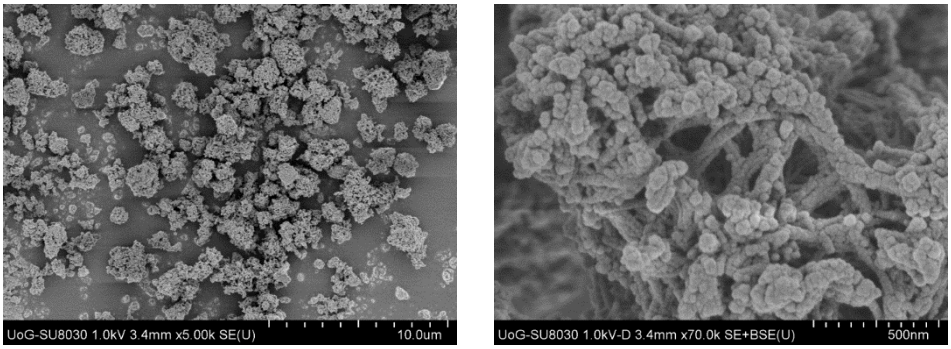

Figure 1. SEM images of MLTUM-Fe_2O_3

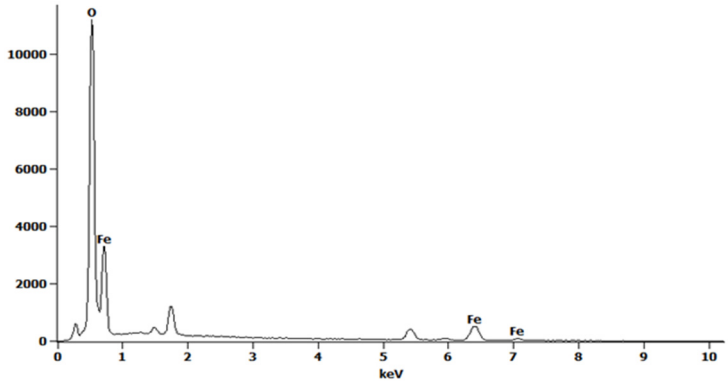

Figure 2. EDX spectra of MLTUM-Fe_2O_3

Thermogravimetric analysis (TGA) of MLTUM-Fe_2O_3 was carried out up to 700ºC (Fig. 3). The weight loss was observed to take place in two steps. The first weight loss is computed to be 20.76% at 375ºC. This weight loss in the temperature range 0–375ºC may be attributed to the loss of physisorbed and interstitial water. Further warming over 400ºC leads to a slight loss of weight (0.55%). The results of TG analysis show that the total weight loss is 21.31%. This confirms that a chemical transformation of hydroxide into the oxide has occurred.

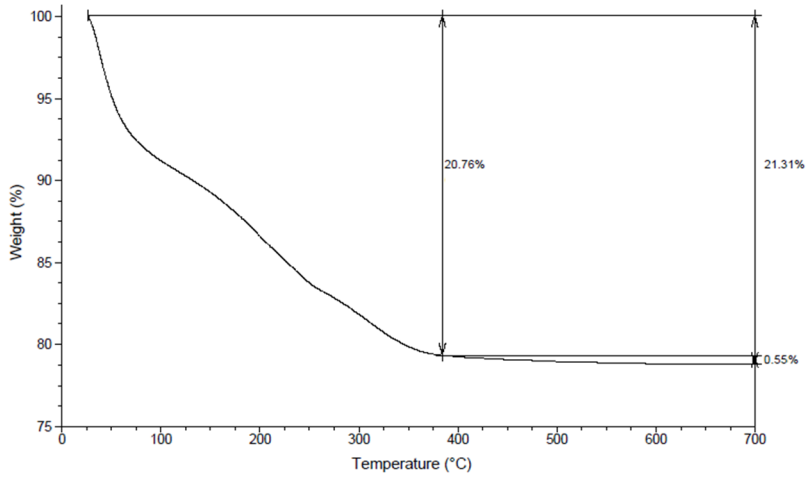

Figure 3. TGA of MLTUM-Fe_2O_3

Fig. 4. shows the FTIR spectra of MLTUM-Fe_2O_3. The band centred at 3416.23 and 1633.39 cm^{-1} are ascribed to O–H bonding stretching and bending vibrational modes [39]. It suggested the presence of very small amount of free and sorbed water on the surface of the sample. As shown in figure, a peak at 530.32 and 451.25 cm^{-1} is ascribed to the stretching between iron and oxygen in Fe_2O_3 [40].

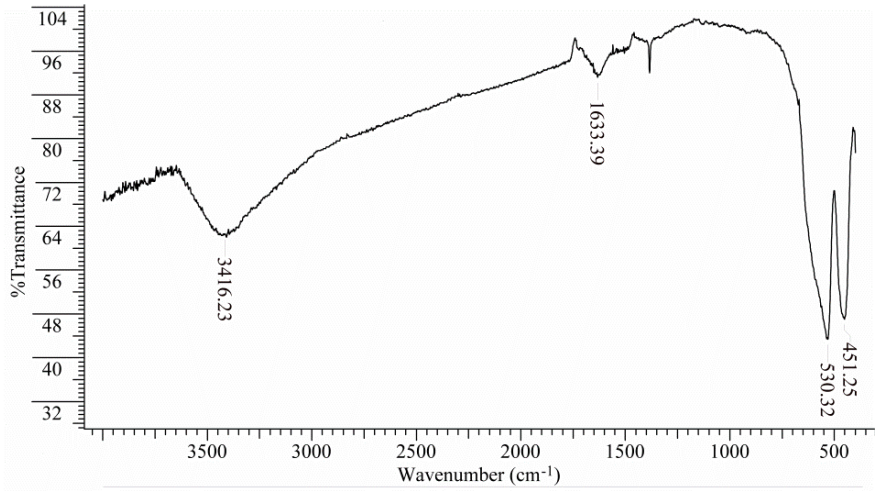

Figure 4. FTIR spectra of MLTUM-Fe_2O_3

Determination of the point of zero charge

The point of zero charge (PZC) is an important parameter that indicates the linear range of pH sensitivity and the sorption ability of the surface. The PZC value was determined by a simplified mass potentiometric titration method [41,42]. pH of solution after sorption vs pH before sorption is plotted and PZC value of MLTUM-Fe_2O_3 nanoparticle is found to 2.78.

Effects of contact time

Results on Fig. 5. indicates the effect of contact time on the removal efficiency and here it is followed that the rapid sorption of RB 19 took place within 5 min. Subsequently, sorption became slow and almost reached equilibrium within 15 min. However, the experimental data were measured at 180 min to make sure that full equilibrium was attained.

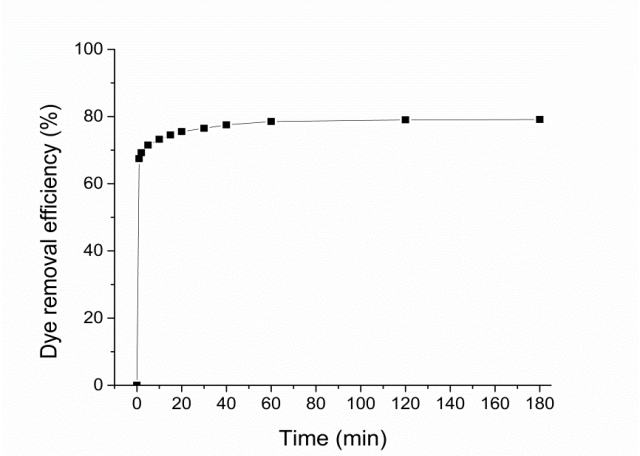

Figure 5. Effect of contact time on RB 19 removal using MLTUM-Fe_2O_3. Initial dye concentration 100 mg dm^{-3}, sorbent dose = 0.5 g dm^{-3}, native pH, temperature = 25 ± 0.5ºC

Effect of sorbent dosage

To optimize the minimum dosage required for bringing down the RB 19 level, the dosage of sorbent was varied from 0.1 g dm^{-3} to 1 g dm^{-3}. The removal efficiency of RB 19 with different sorbent dosage is shown in Fig. 6. The percentage removal of RB 19 significantly increased with sorbent dosage. In all the subsequent experiments 0.5 g dm^{-3} of sorbent was fixed as the optimum dosage.

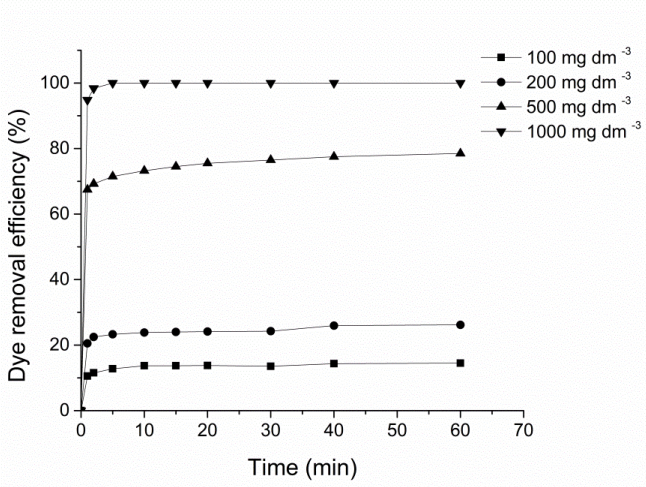

Fig. 6. Effect of sorbent dosage on RB 19 removal using MLTUM-Fe_2O_3. Initial dye concentration 100 mg dm^{-3}, native pH, temperature = 25 ± 0.5ºC

Effect of initial dye concentration

The effect of initial dye concentration was studied in the concentration range 1–500 mg dm^{-3} at native pH value. It was evident that for lower initial concentrations of RB 19, the sorption was very fast (Fig. 7). The removal of RB 19 decreased with increase in initial dye concentration and took longer time to reach equilibrium.

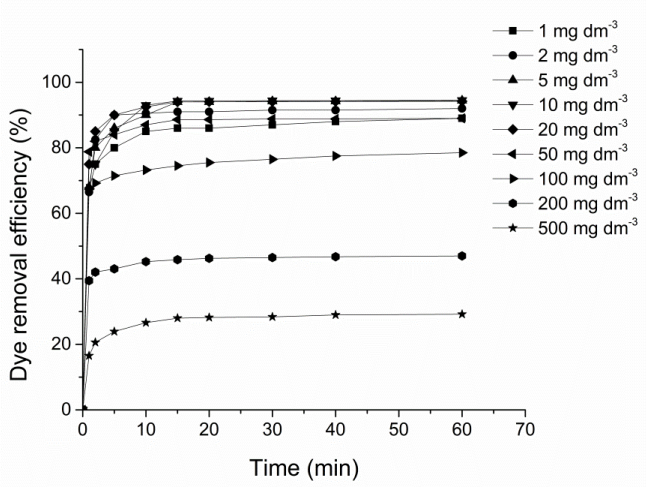

Fig. 7. Effect of initial dye concentration on RB 19 removal using MLTUM-Fe_2O_3. Sorbent dose = 0.5 g dm^{-3}, native pH, temperature = 25 ± 0.5ºC

Effect of pH

To study the effect of pH on the sorption of RB 19, experiments were carried out in the pH range of 2–11. Anionic dye sorption is favoured at pH < pH_{pzc} where the surface becomes positively charged [43]. It can be observed that the sorption of RB 19 increases in the acidic medium (Fig. 8). Although the dye removal efficiency decreased from 89.35% to 14.90 when pH was raised from 2 to 11. This can be explained on the basis of the point of zero charge [44]. Therefore, the surface of MLTUM-Fe_2O_3 is positively charged below the PZC and negatively charged above the PZC.

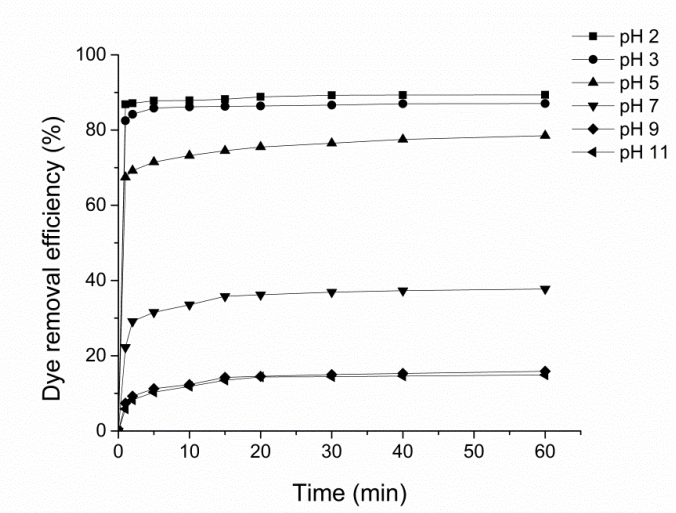

Figure 8. Effect of pH on RB 19 removal using MLTUM-Fe_2O_3. Initial dye concentration 100 mg dm^{-3}, sorbent dose = 0.5 g dm^{-3}, temperature = 25 ± 0.5ºC

Sorption kinetics

The rate of sorption was determined by studying the sorption kinetics at nine different initial RB 19 concentrations (1, 2, 5, 10, 20, 50, 100, 200 and 500 mg dm^{-3}) at optimum sorbent dose. It was observed that RB 19 removal increased with the lapse of time and the rate was initially rapid, after which the rate slowed down as the equilibrium approached. The values of the kinetic models parameters calculated non-linearly are given in Table 1. The experimental data showed that pseudo-second-order model better fitted experimental data than pseudo-first-order model.

Table 1. Pseudo-first order and pseudo-secoond-order kinetic parameters for the RB 19 dye sorption onto MLTUM-Fe_2O_3

C_0 (mg dm^{-3})	1	2	5	10	20	50	100	200	500
q_e, exp (mg g^{-1})	1.800	3.725	9.448	18.977	37.774	89.341	157.224	189.014	271.002
Pseudo-first-order model									
q_e, cal (mg g^{-1})	1.720	3.647	9.242	18.548	37.245	87.576	150.492	183.159	259.704
k_1 (min^{-1})	1.367	1.271	1.221	1.092	1.084	1.052	1.012	0.953	0.801
R^2	0.983	0.995	0.987	0.979	0.995	0.993	0.984	0.988	0.969
Pseudo-second-order model									
q_e, cal (mg g^{-1})	1.766	3.731	9.506	19.139	37.982	88.819	153.093	186.585	273.015
k_2 (min^{-1})	1.656	0.772	0.263	0.110	0.103	0.091	0.039	0.026	0.004
R^2	0.997	0.996	0.999	0.997	0.999	0.998	0.994	0.997	0.994

Since neither the pseudo-first-order nor pseudo-second-order model can identify the diffusion mechanism, the kinetic results were further analyzed by intraparticle diffusion model [45]. Values of the parameters of the intraparticle diffusion model are shown in Table S4 in Supplementary.

Based on k_{id1} and k_{id2} values it can be concluded that film diffusion is more efficient than intraparticle diffusion. The calculated intra-particle diffusion rate constants k_{id3} (Table S4) increased with increasing initial RB 19 which can be related to faster diffusion.

Chrastil's diffusion model describes sorption kinetics in diffusion-controlled systems. The original equation for Chrastil's diffusion model is presented in detail in paper by Chrastil (1990) [46]. The parameters of the model were determined by a non-linear regression analysis of experimental data and given in Table S5 in Supplementary material section. The results obtained for the diffusion resistance coefficient show that *n* values decrease from 0.652 to 0.051 (Table S5) for initial RB 19 concentration from 1 up to 500 mg dm^{-3}, meaning that the sorption rate is strongly limited by the diffusion [47].

Sorption isotherms

In this work, different equilibrium models of two (Langmuir, Freundlich, Temkin, and Dubinin-Radushkevich) and three (Sips) parameters were evaluated to fit the experimental MLTUM-Fe_2O_3 sorption of RB 19 isotherm. Fig. S6 in Supplementary material section shows the comparison of different isotherms studied at 25ºC. The isotherm parameters of all the above-mentioned models, along with their corresponding r^2 values are presented in Table 2.

Table 2. Characteristic parameters of different isotherm models for RB 19 sorption for the RB 19 dye sorption onto MLTUM-Fe_2O_3

Equilibrium model	Parameter	Value
Langmuir isotherm	K_L (dm^3 mg^{-1})	0.088
	q_m (mg g^{-1})	241.779
	R^2	0.970
Freundlich isotherm	K_F, (dm^3 g^{-1})$^{1/n}$	43.212
	n	3.171
	R^2	0.952
Tempkin isotherm	K_T (dm^3 mg^{-1})	5.082
	b (J mol^{-1})	31.823
	R^2	0.969
Dubinin-Radushkevich isotherm	q_{DR} (mg g^{-1})	207.022
	K_{DR} (mol^2 kJ^{-2})	$5.024 \cdot 10^{-6}$
	E (J mol^{-1})	315.557
	R^2	0.909
Sips isotherm	q_m (mg g^{-1})	299.383
	K_S (dm^3 mg^{-1})	0.126
	n	1.578
	R^2	0.988

Langmuir isotherm

The Langmuir isotherm [48] is often used to describe the adsorption in homogeneous surfaces based on the assumptions that monolayer adsorption occurs on uniformly energetic adsorption sites with no interactions between adsorbate molecules.

The highest correlation factors ($R^2 > 0.97$) of Langmuir model for RB 19 indicates that the Langmuir model gives the best fit to the experimental data and so the nature of sorption of dyes on the sorbents is more compatible

with Langmuir assumptions and imply that sorption of investigated pollutant on the sorbent is mono-layer and after saturation of this layer no further sorption took place. The maximum RB 19 sorption capacity determined from the Langmuir isotherm model was 241.77 mg g^{-1} (Table 2), which is consistent with the experimental value (271.002 mg g^{-1}).

Freundlich isotherm

The Freundlich isotherm [49] is used for adsorption which involves system with heterogeneous surface energy. It is assumed that the stronger binding sites are occupied first and that the binding strength decreases with the increasing degree of site occupation.

Differences between the monolayer (chemisorption) and multilayer (physisorption) process can be detected by applying the Freundlich model. From the data in Table 2, that value of $1/n = 0.315$ while $n = 3.171$ indicating that the sorption of RB 19 onto MLTUM-Fe_2O_3 is favourable, as noted in the previous adsorption works [50–53]. These values also suggest formation of an almost homogeneous surface.

Temkin isotherm

The Temkin isotherm assumes that the heat of sorption of all the molecules in a layer decreases linearly due to sorbent–sorbate interactions and that sorption is characterized by a uniform distribution of binding energies, up to some maximum binding energy. The original non-linear equation is presented in paper by Temkin and Pyzhev (1940) [54]. The relatively high value of parameter b (31.8232), indicated that there is a significant ionic interaction between RB 19 and MLTUM-Fe_2O_3 sorbent and suggested predominance of chemical sorption.

Dubinin–Radushkevich isotherm

Dubinin–Radushkevich model is used to distinguish between physisorption and chemisorption and also to assess the mechanism of RB 19 sorption on MLTUM-Fe_2O_3. Values q_{DR}, K_{DR} and ε should be determinate from a non-linear plot of q_e versus C_e. Radushkevich (1949) [55] and Dubinin (1965) [56] have reported that the characteristic sorption curve is related to the porous structure of the sorbent. According to the calculated E value, which was 315.557 J mol^{-1}, physical sorption can be involved in RB 19 sorption onto MLTUM-Fe_2O_3. Considering determination coefficient value ($R^2 = 0.909$), it can be concluded that the D-R model doesn't fit well with experimental data (Table 2).

Sips isotherm

The Sips isotherm [57] is a combined form of Langmuir and Freundlich expressions used for predicting the heterogeneous adsorption systems and circumventing the limitation of the rising adsorbate concentration associated with Freundlich isotherm model. The relatively high value of parameter *n* (Table 2) indicates that the Langmuir will be preferable isotherm. This is consistent with the results obtained for other isotherms.

Desorption of RB19 and reused of MLTUM-Fe_2O_3 nanosorbent

Regeneration and reusability of sorbents is an important factor for industrial and practical applications because of the reduction of the need for new amount of sorbent and lowering of synthesis costs of the sorbent materials. It was found that for MLTUM-Fe_2O_3, the removal efficiency (*RE* %) decreased from 78.59% to 75.40% in the first three cycles and then reached 72.47% in the fourth cycle and the fifth cycle reached 70.32%. The maximum desorption efficiency by NaOH was obtained after 15 min and amounted about 82% in the first desorption cycle. In the next cycles desorption efficiency by using NaOH was higher than 92%. The minor decrease of the sorption capacity can be attributed to the loss of the sorbents in the sorption desorption processes and the irreversible binding (chemisorption) of RB19 on MLTUM-Fe_2O_3. Desorption of RB19 using NaCl solution was very low with *DE* % of 21.78%. Therefore, the MLTUM-Fe_2O_3 can be reutilized, with previously desorption using NaOH.

CONCLUSION

The Fe_2O_3 nanoparticles have been synthesized using simple and fast modified low-temperature urea method and successfully characterized by BET, SEM, EDX, XRD, TGA and FTIR techniques. MLTUM-Fe_2O_3 can be used as potential sorbent for the removal RB 19 from water with a maximum sorption capacity of 271.00 mg g^{-1} for dye at room temperature. The kinetic data shows that the present system follows pseudo-second-order model. Equilibrium sorption data fit better to Langmuir followed by Sips, Tempkin, Freundlich and Dubinin-Radushkevich sorption models, respectively. Hence, this study could provide a simple route to synthesize a cost-effective nanostructured Fe_2O_3 sorbent for dyes removal in environmental treatment.

EXPERIMENTAL

Materials

Ferric nitrate $Fe(NO_3)_3 \cdot 9\ H_2O$ (Sigma Aldrich, USA) and urea $(NH_2)_2CO$ (Merck, Germany) with 99% and 99.5% purities respectively, were employed as the starting materials. The dye Reactive Blue 19 (RB 19) was obtained from Sigma Aldrich (USA) and used without further purification. The properties and molecular structure of RB 19 are shown in Table S2 in Supplementary material section.

Synthesis

Iron oxide nanoparticles was synthesized by a modified low-temperature urea method. The effect of the fuel in controlling particle size and microstructure of the product under different fuel-to-oxidant ratios is investigated by a few scientists [37,38]. Initially, three aqueous solutions of the ferric nitrate nonahydrate $Fe(NO_3)_3 \cdot 9\ H_2O$ and urea $(NH_2)_2CO$ with Fe:urea molar ratio 1:2.5, 1:5 and 1:7.5 were added to three flasks with reflux condenser, which were maintained at 90ºC for 3 h. After that the suspensions were cooled to room temperature, filtered and washed with hot deionized water for effective removal of ions. The final products were dried at 100ºC for 10 h. For further research, the iron oxide obtained with molar ratio 1:2.5 was used because with the further increase in the amount of urea there was no increase in the sorption of the material. The material with Fe:urea molar ratio 1:2.5 will be marked as MLTUM-Fe_2O_3 further in the text.

Characterization

The structure of MLTUM-Fe_2O_3 was determined by X-ray powder diffraction (XRD). Data were collected with a Siemens D5000 X-ray Diffractometer in theta-theta geometry in reflection mode with Co Kα. Data collection was between 20-80º 2θ, step size of 0.02º. For SEM-EDX analysis samples were attached to aluminum stubs using Leit-C carbon cement. A Hitachi SU8030 cold FEG-SEM was used for imaging the samples with Thermo-Noran NSS system 7 ultra-dry x-ray detector for semi-quantitative EDX analysis (Thermo Scientific NORAN System 7, USA). An infrared spectrum of MLTUM-Fe_2O_3 was obtained using a Fourier transform infrared spectrometer (Bomem Hartmann & Braun MB-100 spectrometer).

The specific surface area was evaluated by the BET method using N_2 adsorption. A full gas sorption isotherm was run on a Micromeritics Gemini 5 Surface Area Analyser. The pore size distribution was calculated from the desorption branch of the isotherm by the Barrett, Joyner, and Halenda (BJH)

method. Thermogravimetric analysis (TGA) was performed using TGA Q5000 (TA Instruments, USA). The sample was heated in air at a flow rate of 25 cm^3 min^{-1} from ambient temperature to 600ºC in aluminum pan, at a heating rate of 2ºC min^{-1}.

Sorption experiments

Studies on the sorption of dye RB 19 by MLTUM-Fe_2O_3 were carried out in batch conditions. 100 cm^3 of each of working dye solution was contacted with 0.05 g sorbent, stirred at 250 rpm, at room temperature 25.0 ± 0.5°C. Aliquots of solutions (5.0 cm^3) were withdrawn at desired time intervals and the sorbent was removed immediately by filtration through a 0.20 μm regenerated cellulose membrane filter (Agilent Technologies, Germany). Absorbance at 592 nm was measured using a UV/vis spectrophotometer Shimadzu UV-1800 PC (Shimadzu, Japan). The amount of dye sorbed q_t (mg g^{-1}) was determined by using the following equation 1:

$$q_t = \frac{(c_i - c_t)}{m} \tag{1}$$

The percentage of removal was evaluated using equation 2:

$$\text{RE}\ (\%) = \left(1 - \frac{c_t}{c_0}\right) \times 100 \tag{2}$$

where c_0 and c_t are the initial and final concentrations of the dye in solution (mg dm^{-3}), V is the solution volume (dm^3) and m is the mass of the sorbent (g).

Desorption of RB19 and reused of MLTUM-Fe_2O_3 nanosorbent

In order to investigate the reusability performance of the MLTUM-Fe_2O_3 nanosorbent, five successive sorption–desorption (regeneration) cycles were performed. In the adsorption test, 0.05 g of MLTUM-Fe_2O_3 was loaded with 100 cm^3 of RB19 solution with concentration of 100 mg dm^{-3} and stirred for 180 min. To regenerate the adsorbent, the used MLTUM-Fe_2O_3 was contacted with 100 cm^3 of desorption solutions (0.1M NaOH and 1M NaCl), with stirring for 1 h. The desorption efficiency (*DE* %) was calculated as follows:

$$\text{DE}\ (\%) = \left(\frac{m_{\text{desorbedRB 19}}\,[mg]}{m_{\text{previously sorbed}}\,[mg]}\right) \times 100 \tag{3}$$

ACKNOWLEDGEMENTS

The authors would like to acknowledge financial support from the Ministry of Education, Science and Technological Development of the Republic of Serbia (Agreement No 451-03-68/2020-14/200124).

REFERENCES

1. C. O'Neill; F.R. Hawkes; D.L. Hawkes; N.D. Lourenco; H.M. Pinheiro; W. Delee; *Chem. Technol. Biot*., **1999**, *74*, 1009-1018.
2. I. Arslan-Alaton; B.H. Gursoy; J.E. Schmidt; *Dyes Pigm.*, **2008**, *78*, 117-130.
3. J. (Ed.) Shore; *Dyeing with Reactive Dyes*, Formerly of BTTG-Shirley and ICI (now Zeneca), Manchester, UK, **1995**.
4. P. (Ed.) Gregory; *Toxicology of Textile Dyes*, Heriot-Watt University, UK, **2007**.
5. Y. Verma; *Toxicol. Ind. Health*, **2011**, *27*, 41-49.
6. J.E.B. McCallum; S.A. Madison; S. Alkan; R.L. Depinto; R.U. Rohas Wahl; *Environ. Sci. Technol*., **2000**, *34*, 5157-5164.
7. M. Siddique; R. Farooq; Z.M. Khan; Z. Khan; S.F. Shaukat; *Ultrason. Sonochem*., 2011, *18*, 190-196.
8. A. Dabrowski; *Adv. Coll. Interface Sci*., **2001**, *93*, 135-224.
9. T. Robinson; G. McMullan; R. Marchant; P. Nigam; *Bioresour. Technol*., **2001**, *77*, 247-255.
10. O. Aktas; F. Cecen; *Int. Biodeterior. Biodegrad*., **2007**, *5*9, 257-272.
11. E. Hosseini Koupaie; M.R. Alavi Moghaddam; S.H. Hashemi; *Int. Biodeterior. Biodegrad*., **2012**, *71*, 43-49.
12. J. Zolgharnein; N. Asanjarani; T. Shariatmanesh; *Int. Biodeterior. Biodegrad*., **2013**, *85*, 66-77.
13. R.S. Juang; R.L. Tseng; F.C. Wu; S.H. Lee; *J. Chem. Technol. Biot*., **1997**, *70*, 391-399.
14. K.Y. Ho; G. McKay; K.L. Yeung, *Langmuir*, **2003**, *19*, 3019-3024.
15. Q.Y. Sun; L.Z. Yang; *Water Res*., **2003**, *37*, 1535-1544.
16. M. Valix; W.H. Cheung; G. McKay; *Langmuir*, **2006**, *22*, 4574-4582.
17. B.H. Hameed; A.A. Ahmad; N. Aziz; *Chem. Eng. J*., **2007**, *133*, 195-203.
18. I.A. W. Tan; B.H. Hameed; A.L. Ahmad; *Chem. Eng. J*., **2007**,*127*, 111-119.
19. A. Mittal; L. Kurup; J. Mittal; *J. Hazard. Mater*., **2007**, 146, 243-248.
20. I.A. W. Tan; A.L. Ahmad; B.H. Hameed; *J. Hazard. Mater.*, **2008**, *154*, 337-346.
21. E. Eren; B. Afsin; *Dyes Pigments*, **2008**, *76*, 220-225.
22. A.P. Vieira; S.A.A. Santana; C.W.B. Bezerra; H.A.S. Silva; J.A.P. Chaves; J.C.P. de Melo; E.C. da Silva Filho; C. Airoldi; *J. Hazard. Mater*., **2009**, *166*, 1272-1278.

23. B.K. Nandi; A. Goswami; M.K. Purkait; *Appl. Clay. Sci.*, **2009**, *42*, 583-590.
24. O. Gok; A.S. Ozcan; A. Ozcan; *Appl. Surf. Sci.*, **2010**, *256*, 5439-5443.
25. A.R. Khataee; F. Vafaei; M. Jannatkhah; *Int. Biodeterior. Biodegrad*., **2013**, *83*, 33-40.
26. R. Darvishi Cheshmeh Soltani; A.R. Khataee; M. Safari, S.W. Joo; *Int. Biodeterior. Biodegrad*., **2013**, *85*, 383-391.
27. N.K. Nga; P.T.T. Hong; T.D. Lam; T.Q. Huy; *J. Colloid. Interf. Sci*., **2013**, *398*, 210-216.
28. U. A. Isah; G. Abdulraheem; S. Bala; S. Muhammad; M. Abdullahi; *Int. Biodeterior. Biodegrad*., **2015**, *102*, 265-273.
29. D.C. dos Santos; M.A. Adebayo; E.C. Lima; S.F.P. Pereira; R. Cataluna; C. Saucier; P.S. Thue; F.M. Machado; *J. Braz. Chem. Soc*., **2015**, *26*, 924-938.
30. S. Karimifard; M. R. A. Moghaddam; *Process Saf. Environ. Prot*., **2016**, *99*, 20-29.
31. N.K. Nga; H.D. Chinh; P.T.T. Hong; T.Q. Huy; *J. Polym. Environ*., **2017**, *25*, 146-155.
32. G. Ciobanu; S. Barna; M. Harja; *Arch. Environ. Protec*., **2016**, *42*, 3-11.
33. Y. Liu; M. Yan; Y. Geng; J. Huang; *Appl. Sci.*, **2016**, *6*, 232-245.
34. M. Shanehsaz; S. Seidi; Y. Ghorbani; S.M.R. Shoja; S. Rouhani; *Spectrochim. Acta., Part* A, **2015**, *149*, 481-486.
35. G. Moussavi; M. Mahmoudi; *J. Hazard. Mater*., **2009**, *168*, 806-812.
36. Z.M. Khoshhesab; M. Ahmadi; *Desalination Water Treat*., **2016**, *57*, 20037-
37. R.D. Purohit; B.P. Sharma; K.T. Pillai; A.K.Tyagi; *Mater. Res. Bull*., **2001**, *36*, 2711-2721.
38. J.C. Toniolo; M.D. Lima; A.S. Takimi; C.P. Bergmann; *Mater. Res. Bull*., **2005**, *40*, 561-571.
39. L.M. Song; S.J. Zhang; *Colloids Surf. A: Physicochem. Eng. Asp*., **2010**, *360*, 1-5.
40. R.M. Cornell; U. Schwertmann; The Iron Oxides: Structure, Properties, Reactions, Occurrences and Uses, Wiley-VCH, New York, **2003**.
41. P. Balderas-Hernandez; J.G. Ibanez; J.J. Godinez-Ramirez; F. Almada-Calvo; *Chem. Educator*, **2006**, *11*, 267-270.
42. J.G. Ibanez; M. Hernandez-Esparza; C. Doria-Serrano; A. Fregoso-Infante; M.M. Singh; *Environmental Chemistry: Microscale Laboratory Experiments*, Springer, New York, **2008**.
43. D. Savova; N. Petrov; M. Yardim; E. Ekinci; T. Budinova; M. Razvigorova; V. Minkova; *Carbon*, **2003**, *41*, 1897-1903.
44. S. Al-Qaradawi; S. R. Salman; *J. Photochem. Photobiol. A: Chem.*, **2002**, *148*, 161-168.
45. W.J. Jr. Weber; J.C. Morris; *J. Sanit. Eng. Div*., 1964, *89*, 31-60.
46. J. Chrastil; *Text. Res. J*., **1990**, *60*, 413-416.
47. F. Carrillo; M.J. Lis; X. Colom; M. Lopez-Mesas; J. Valldeperas; *Process Biochem*., **2005**, *40*, 3360-3364.
48. I. Langmuir; *J. Am. Chem. Soc*., **1916**, **38**, 2221-2295.
49. H.Z. Freundlich; *J. Phys. Chem*., **1906**, *57A*, 385-470.
50. A.A. Ismaiel; M.K. Aroua; R. Yusoff; *Chem. Eng. J*., **2013**, *225*, 306-314.

51. H.K. Boparai; M. Joseph; D.M. O'Caroll; *J. Hazard. Mater*., **2011**, *186*, 458-465.
52. G. Vazquez; M. Sonia Freire; J. Gonzalez-Alvarez; G. Antorrena; *Desalination*, **2009**, 249, 855-860.
53. N. Asasian; T. Kaghazchi; M. Soleimani; *J. Ind. Eng. Chem*., **2012**, *18*, 283-289.
54. M.I. Temkin; V. Pyzhev; *Acta Physicochim.*, **1940**, *12*, 217-222.
55. L.V. Radushkevich; *Zhurnal Fizicheskoi Khimii* **1949**, *23*, 1410-1420.
56. M.M. Dubinin; *Chem. Rev.*, **1960**, *60*, 235-266.
57. R. Sips; *J. Chem. Phys*., **1948**, *16*, 490-495.